International Journal of Technology

http://ijtech.eng.ui.ac.id

Research Article

Development of Array Triangular Microstrip Antenna for Circularly Polarized-Synthetic Aperture Radar

Muhammad Fauzan Edy Purnomo[1*], Vita Kusumasari[2], Akhmad Zainuri[1], Fakhriy Hario Partiansyah[1], Sigit Kusmariyanto[1], Dwi Fadila Kurniawan[1], Rahmadwati Rahmadwati[1], Muhammad Aziz Muslim[1], Hadi Suyono[1], Rini Nur Hasanah[1], Khairul Anam[3], Nurhayati Nurhayati[4], Puput Dani Prasetyo Adi[5], Bambang Setiadi[5], Farohaji Kurniawan[6], Joshapat Tetuko Sri Sumantyo[7]

[1]Department of Electrical Engineering, Universitas Brawijaya, Malang 65145, Indonesia

[2]Department of Mathematics, Universitas Negeri Malang, Malang 65145, Indonesia

[3]Department of Mechanical Engineering, Universitas Brawijaya, Malang 65145, Indonesia

[4]Department of Electrical Engineering, Universitas Negeri Surabaya, Surabaya 60231, Indonesia

[5]Telecommunication Research Center of the National Research and Innovation Agency, Bandung 40135, Indonesia

[6]Aeronautical Technology Research Center, OR Aerospace, Cikoleang, Bogor 16350, Indonesia

[7]Center for Environmental Remote Sensing, Chiba University, Chiba 2638522, Japan

[*]Corresponding author: mfauzanep@ub.ac.id; Tel.: +62-341554166; Fax: +62-341554166

Abstract: Circularly Polarized Synthetic Aperture Radar is an active remote sensing system that employs left- and right-handed circular polarization to enhance Earth observation capabilities. By operating in the *C*, *S*, and *L* frequency bands, Circularly Polarized Synthetic Aperture Radar enables the generation of axial ratio, ellipticity, and tilt angle images, thereby improving information extraction and overcoming conventional Synthetic Aperture Radar limitations such as high-power consumption, Faraday rotation sensitivity, backscatter distortion, and low target discrimination. In this study, we propose and investigate triangular microstrip array antennas as the core radiating elements for Circularly Polarized Synthetic Aperture Radar applications in the *L*-bands and *C*-bands. Designed for integration into Low Earth Orbit microsatellites and Unmanned Aerial Vehicles, these antennas provide notable advantages including compactness, light weight, conformability, cost-effectiveness, and ease of integration with other circuits. Numerical simulations, supported by partial experimental validation, confirm that the proposed antennas achieve adequate gain, axial ratio bandwidth, beamwidth, and efficiency. These results demonstrate that triangular microstrip arrays can fulfill the technical requirements for Circularly Polarized Synthetic Aperture Radar implementation on Low Earth Orbit and Unmanned Aerial Vehicle platforms, offering a promising solution for advanced, low-cost remote sensing systems.

Keywords: Circularly polarized synthetic aperture radar; Low earth orbit; Microstrip array antenna; Remote sensing; Unmanned aerial vehicle

1. Introduction

Radar imaging systems can generally be classified into two major categories: scanning-based displays and side-looking observation modes. Plan-Position Indicator (PPI) radar is mainly used for monitoring air and maritime traffic, whereas side-looking radar configurations are widely applied in remote sensing applications. In this context, remote sensing radar systems are commonly divided into Real Aperture Radar (RAR), also known as Side-Looking Airborne Radar (SLAR), and Synthetic Aperture Radar (SAR), which provides enhanced imaging resolution through signal processing techniques. SAR has become one of the most important active microwave sensing technologies for Earth observation because of its capability to operate in day-and-night and all-

https://doi.org/10.14716/ijtech.v17i3.8398
Received July 2025; Revised February 2026; Accepted April 2026

weather conditions. Recent developments in spaceborne polarimetric SAR systems also confirm the continued importance of circularly polarized and polarization-sensitive radar architectures for remote-sensing missions (Jiao et al., 2025).

In airborne SAR platforms such as Unmanned Aerial Vehicles (UAVs), the antenna beam is often tilted due to the forward motion of the vehicle. One effective approach to control and adjust the beam direction is through the excitation of higher-order resonant modes in microstrip-array configurations. While a single antenna element typically radiates mainly through its dominant mode, array configurations with suitable feeding networks can support more flexible beam control and gain enhancement (Tran-Huy and Pham-Danh, 2025). This issue is particularly relevant for UAV-based systems, where compactness, low profile, beam control, and lightweight implementation are all essential design requirements. Recent reviews on UAV antennas likewise emphasize the trade-off among platform limitations, polarization control, and radiation performance (Reis et al., 2025).

Circular polarization (CP) is especially beneficial in SAR applications because it improves target discrimination and reduces the influence of polarization mismatch and propagation effects such as Faraday rotation. The beam direction in CP microstrip antennas can deviate from broadside and can be tailored through the feeding configuration, coupling mechanism, and radiatingelement geometry, which affect the excitation of orthogonal modes required for circularly polarized tilted-beam radiation (Li et al., 2024). This phenomenon occurs because the feed structure interacts with perturbation segments that support circularly polarized radiation. More recent studies have also shown that beam-tilted circularly polarized array antennas are highly relevant for UAV-oriented platforms, where directional control and compact implementation are required (Park et al., 2024). For UAV-based SAR systems, the antenna beam is commonly oriented perpendicular to the flight path so that range resolution is formed in the direction orthogonal to the observation track, while azimuth resolution is aligned with the platform motion. In practice, this means that antenna characteristics remain critical to image quality, because SAR processing mainly enhances azimuth resolution, whereas the antenna itself strongly affects coverage, radiometric behavior, and polarization performance.

Among the candidate radiators for compact SAR payloads, microstrip antennas are attractive because of their low profile, light weight, low fabrication cost, and ease of integration with microwave circuitry. In particular, triangular microstrip radiators have been studied extensively for circularly polarized radar and SAR-related applications. Baharuddin et al. (2009) demonstrated an equilateral triangular microstrip antenna for *L*-band CP-SAR and reported a 3-dB axial-ratio bandwidth of about 0.58% (7.4 MHz), thereby confirming the feasibility of triangular CP radiation at the element level. Delaune et al. (2006) reported a circularly polarized rounded-off triangular microstrip line array antenna with a minimum gain of 6.6 dBic and a maximum axial ratio of 2.9 dB, showing that triangular CP arrays can also be realized in directional array environments. More recently, Purnomo et al. (2021) developed a two-patch stacked triangular truncated microstrip antenna for CP-SAR and reported approximately 7.24 dBic gain, 1.99 dB axial ratio, and 90.13% radiation efficiency. These studies clearly demonstrate the feasibility of triangular CP antennas and arrays; however, they also indicate that much of the prior work is centred on concept validation, limited array scales, or partial performance achievements rather than on full compliance with broader CP-SAR system requirements (Jiao et al., 2025).

For CP-SAR implementation on UAV and Low Earth Orbit (LEO) microsatellite platforms, however, the antenna is not only required to generate circular polarization, but also to satisfy several performance metrics simultaneously, including sufficient gain, acceptable axial ratio, high radiation efficiency, and suitable azimuth and range beamwidths, as summarized in Table 1 (Yohandri et al., 2011). These requirements are challenging because they are interdependent. Increasing gain usually requires a larger aperture and more array elements, but this also increases feed-network complexity, conductor loss, and overall antenna size. Similarly, improving the purity of circular polarization through perturbation or feeding optimization can affect impedance matching, bandwidth, and radiation stability. The challenge becomes more

severe in *L*-band because the longer wavelength results in physically larger structures, whereas UAV and microsatellite platforms impose strict limitations on antenna area, payload mass, and mechanical integration (Wahyudi et al., 2025). Recent UAV-oriented CP-SAR antenna developments continue to highlight these same trade-offs between compactness, gain, polarization quality, and platform compatibility (Kashihara et al., 2023; Reis et al., 2025).

In addition to the classical development of triangular microstrip antennas for CP-SAR, recent research has expanded toward wideband circularly polarized arrays, metasurface-assisted bandwidth enhancement, and characteristic-mode-based CP antenna synthesis. Several recent studies from 2022 to 2025 have reported low-profile and high-gain wideband CP antennas using metasurfaces, hybrid metasurface superstrates, and connected or array-based radiators. In parallel, modern SAR system research has increasingly emphasized digital beamforming, scan-on-receive operation, multichannel ambiguity suppression, and improved antenna-pattern characterization for advanced spaceborne SAR systems. Therefore, the present work should be positioned not only against classical triangular CP-SAR antennas, but also against these more recent developments in wideband CP array design and beamforming-oriented SAR antenna systems (Chen et al., 2024; Ding et al., 2023; Dong et al., 2025; Li et al., 2025; Liu et al., 2022).

Therefore, the key research gap is not the absence of triangular CP antennas themselves, but the limited analytical demonstration that compact triangular microstrip arrays can satisfy CP-SAR-oriented system specifications in a balanced manner. In particular, representative earlier triangular CP studies reported gains such as 6.6 dBic and 7.24 dBic, which are sufficient to prove feasibility but remain substantially below the $\geq$15 dBic gain target specified in Table 1, even though their axial-ratio performance is already acceptable. This indicates that the unresolved issue is not merely achieving circular polarization, but achieving high gain together with acceptable axial ratio, beamwidth, efficiency, and compactness in practical CP-SAR array configurations (Kashihara et al., 2023; Park et al., 2024).

In this study, triangular microstrip antennas are investigated as fundamental radiating elements for circularly polarized synthetic aperture radar (CP-SAR) systems operating in both the *L*- and *C*-bands. The contribution of this work lies in the system-oriented design and evaluation of triangular microstrip array configurations under explicit CP-SAR performance targets for compact UAV and LEO platforms. To realize circular polarization and beam shaping, corporate feeding networks and perturbation-based triangular geometries are employed, while numerical simulations and partial experimental validation are conducted to evaluate the reflection coefficient, gain, axial ratio, beamwidth, and radiation efficiency (Kashihara et al., 2023; Reis et al., 2025). This study aims to determine the extent to which triangular CP arrays can satisfy the practical antenna requirements of compact CP-SAR platforms in both *L*-band and *C*-band implementations (Urata et al., 2019). Recent UAV-borne full CP-SAR antenna developments further support the relevance of this system-level direction (Kashihara et al., 2023; Park et al., 2024).

The remainder of this paper is organized as follows: Section 2 describes the antenna design methodology and simulation approach, Section 3 presents the performance results and discussion, and Section 4 concludes the study with key findings and future perspectives.

2. Methods

The proposed CP-SAR antenna was developed through a staged electromagnetic design procedure followed by selective experimental validation. The main objective was to satisfy the CP-SAR system requirements summarized in Table 1, namely operation at *L*-band/*C*-band, axial ratio below 3 dB, high radiation efficiency, sufficient gain, and beamwidth appropriate for side-looking SAR observation. In this method, the design process is explicitly defined as a parametric optimization workflow, rather than as a global numerical optimization algorithm. This choice is appropriate because the antenna geometry, perturbation structure, and corporate-feed network were refined iteratively through engineering trade-offs among impedance matching, circular polarization quality, gain, and array radiation behavior. The present manuscript frames

the work as a simulation-driven design followed by partial chamber validation, which supports this staged interpretation (Purnomo et al., 2021).

The overall workflow consisted of four stages: (i) single-element triangular patch design, (ii) development of a divider-fed two-element subarray, (iii) scaling into larger array configurations, and (iv) final performance verification. At the element level, an equilateral triangular microstrip patch was adopted as the reference radiator. Circular polarization was produced by introducing truncated-tip perturbations, since such perturbations are known to split the near-degenerate resonant modes and create the orthogonal field components required for circular polarization in equilateral triangular microstrip antennas. In this stage, the principal tuning variables were the patch side length, truncation dimensions, and feed location. The patch side length primarily controlled the resonant frequency, whereas the truncation geometry and feed position were adjusted to minimize the axial ratio while preserving acceptable impedance matching near the target band.

After obtaining a stable single element, the antenna was integrated with a modified 2×1 T-junction corporate feed to form a two-patch subarray. The optimization at this stage was performed by sequential parameter sweep. More specifically, the widths of the microstrip branches, the lengths of the T-junction transitions, the right-angle bend sections, and the short matching segments were varied one group at a time while the remaining parameters were kept near their previously optimized values. The monitored responses were the reflection coefficient, phase consistency between the output branches, and the quality of power distribution to the radiating elements. This procedure was adopted because corporate-fed arrays require nearly equal amplitude and phase excitation to preserve coherent aperture radiation, and equalized feed paths are a standard means of maintaining this condition.

The validated two-patch subarray was then extended into larger 2×4 and 2×8 triangular arrays. At the array level, the primary design variables were inter-element spacing, total feed-line length, junction dimensions, and bend-compensation parameters. Equal electrical path lengths from the input port to each radiating element were preserved to maintain phase coherence across the aperture. During this stage, the simulated observables used as optimization targets were S_{11}, axial ratio, gain, beamwidth, and radiation-pattern stability. The design iteration was terminated when two consecutive sweep cycles produced only negligible improvement in the combined target responses and the main CP-SAR specifications were satisfied or closely approached. Accordingly, the final design should be understood as the result of staged parametric refinement rather than a population-based or gradient-based optimizer.

For electromagnetic analysis, the Method of Moments (MoM) was used to determine the current distribution on the metallic radiating surfaces. In MoM-based antenna analysis, the unknown current is expanded through basis functions and transformed into a solvable matrix system, from which input and radiation characteristics can be extracted. In this work, the C-band reference design and the L-band free-space array configuration were analyzed using the simulation platforms stated in the manuscript; however, the essential methodological point is that both platforms were used as full-wave electromagnetic solvers to support the same staged design workflow (Sarkar et al., 2000).

The substrate selection was also treated as part of the design optimization. In microstrip antennas, substrate thickness and dielectric constant strongly influence impedance bandwidth, radiation efficiency, and surface-wave behavior. A relatively low-permittivity substrate was therefore selected to support stronger fringing fields and more efficient radiation, while the substrate thickness was chosen as a trade-off between bandwidth enhancement and the risk of additional surface-wave loss. This consideration is consistent with established microstrip-antenna design principles and is particularly important for circularly polarized arrays, where stable modal behavior and efficient radiation must be achieved simultaneously (Asfour et al., 2024; Beegum et al., 2024; Wong, 2002).

Experimental validation was performed only for the fabricated eight-patch prototype, and the measured quantity was limited to the input reflection coefficient. Therefore, the 5.5 GHz

array includes partial measurement-based validation through S_{11}, whereas the 1.25 GHz configuration and the extended array results are simulation-based verification. This distinction is now explicitly stated to avoid overclaiming experimental completeness. Thus, the main contribution of this work lies in the staged design and verification of circularly polarized triangular microstrip arrays for CP-SAR applications, rather than in a fully comprehensive measurement campaign for every array configuration (Purnomo et al., 2021).

Table 1 Specification of antenna parameter for CP-SAR system.

No.	Parameter	Specification CP-SAR System
1.	Frequency (GHz)	L-band: 1.25–1.27 GHz; C-band: 5.5
2.	Pulse Band Wide (MHz)	10 to 233.31
3.	Axial Ratio (dB)	≤ 3
4.	Antenna Efficiency (%)	> 80
5.	Gain Antenna (dBic)	≥ 15
6.	Azimuth Beamwidth (°)	≥ 1.08
7.	Range Beamwidth (°)	≥ 15
8.	Antenna size (n × m)	(2×1) (2×4) (2×8)
9.	Polarization (Tx/Rx)	LHCP + RHCP + VV + HH

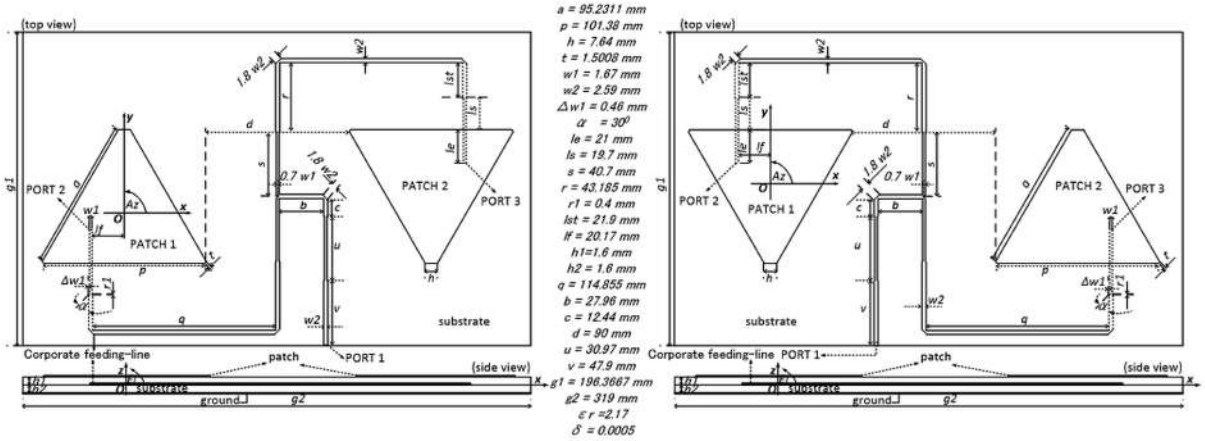

Figure 1 Configuration of LHCP and RHCP array antennas using power divider 2 × 1

2.1 Antenna Geometry and Array Configuration

All triangular patches were designed with identical geometric dimensions. The side length of each equilateral triangular patch is 95.2311 mm, while the overall effective dimension including perturbation parameters is 101.38 mm. Circular polarization is achieved by incorporating truncated-tip perturbation segments with carefully optimized dimensions. The flattened vertices of the triangular patches are deliberately introduced as apex truncations to perturb the patch symmetry and control the current distribution. This feature supports the excitation of orthogonal resonant modes required for circular polarization and also provides additional flexibility for optimizing resonant frequency, axial ratio, and radiation performance in the CP-SAR array.

The corporate feeding network consists of multiple T-junction nodes responsible for uniformly distributing power from the input port to all radiating elements. In the eight-patch configuration, this feed configuration enables the excitation of 2×4 radiating patches with equal path lengths from the input port, total approximately 3.75λ or 219.34 mm. Moreover, in the sixteen-patch configuration fifteen T-junctions are implemented to feed a 2×8 array. To ensure coherent radiation and phase consistency, equal electrical path lengths are maintained from the input port to each radiating element. The total feed-line length is approximately 7.9λ (1286.12

mm) (Basari et al., 2006; Purnomo and Sri Sumantyo, 2011; Purnomo et al., 2014; Purnomo et al., 2015; Purnomo and Kitagawa, 2018; Purnomo et al., 2019; Purnomo et al., 2020; Purnomo et al., 2021; Delfini et al., 2024; Sahana and Sowmya, 2024).

To achieve excitation of the TM_{21} higher-order mode and generate circular polarization, the following design principles were applied Du and Yung, 2002; Chang, 2005; Amr et al., 2017; Delfini et al., 2024; Sahana and Sowmya, 2024; Zhang et al., 2025):

- Proper dimensioning of truncated-tip perturbation elements.
- Minimization of transmission loss in right-angle bends and T-junction transitions.
- Element spacing approximately equal to $\lambda/2$.
- Suppression of unwanted sidelobes to maintain symmetric radiation patterns and stable circular polarization.
- The construction of array eight patches.

2.2 Substrate Selection

The dielectric substrate significantly influences impedance bandwidth, radiation efficiency, and polarization purity. Increasing substrate thickness generally enhances radiation efficiency and bandwidth but may introduce surface wave losses if not properly optimized Deshmukh and Chavali, 2026; Grebennikov, 2011; Ishihara et al., 2002; Chen et al., 2024; Asfour et al., 2024. Conversely, lower dielectric permittivity increases fringing fields and improves radiation characteristics. Which is particularly important for maintaining gain, axial-ratio bandwidth, and radiation efficiency in circularly polarized microstrip antennas (Kedze et al., 2022).

In this work, Nippon Pillar Packing (NPC) H220A was selected as the substrate material. The relative permittivity (ε_r) is 2.17 and the loss tangent (δ) is 0.0009 (Ansoft Corporation, 2001; CST AG, 2016; Deshmukh and Ray, 2020; Du and Yung, 2002; Horng and Alexopoulos, 1993; Mujahidin et al., 2018; Pozar, 2005; Tiwari et al., 2025; Yohandri et al., 2011). The total substrate thickness is 3.2 mm, consisting of two 1.6 mm layers for the radiating patch and corporate feeding network, except the eight-patches array antenna whose total substrate thickness is only 1.6 mm. This configuration was chosen to achieve a balance between bandwidth enhancement, mechanical stability, and high radiation efficiency suitable for UAV and LEO microsatellite deployment.

2.3 Modified Lossless T-Junction Power Divider

A power divider is a multiport microwave network designed to distribute input power from a single port into several output ports with equal amplitude and phase characteristics. Such networks are widely used in corporate-fed antenna arrays to ensure uniform excitation of radiating elements.

One important property of practical power divider structures is reciprocity, meaning that the transmission response between any two ports remains identical regardless of the direction of signal propagation. For a reciprocal device, the scattering matrix satisfies (Deshmukh and Ray, 2020; Grebennikov, 2011; Morini et al., 2024; Purnomo and Kitagawa, 2017):

$$S_{ij} = S_{ji} \tag{1}$$

which indicates that the S-matrix is symmetric.

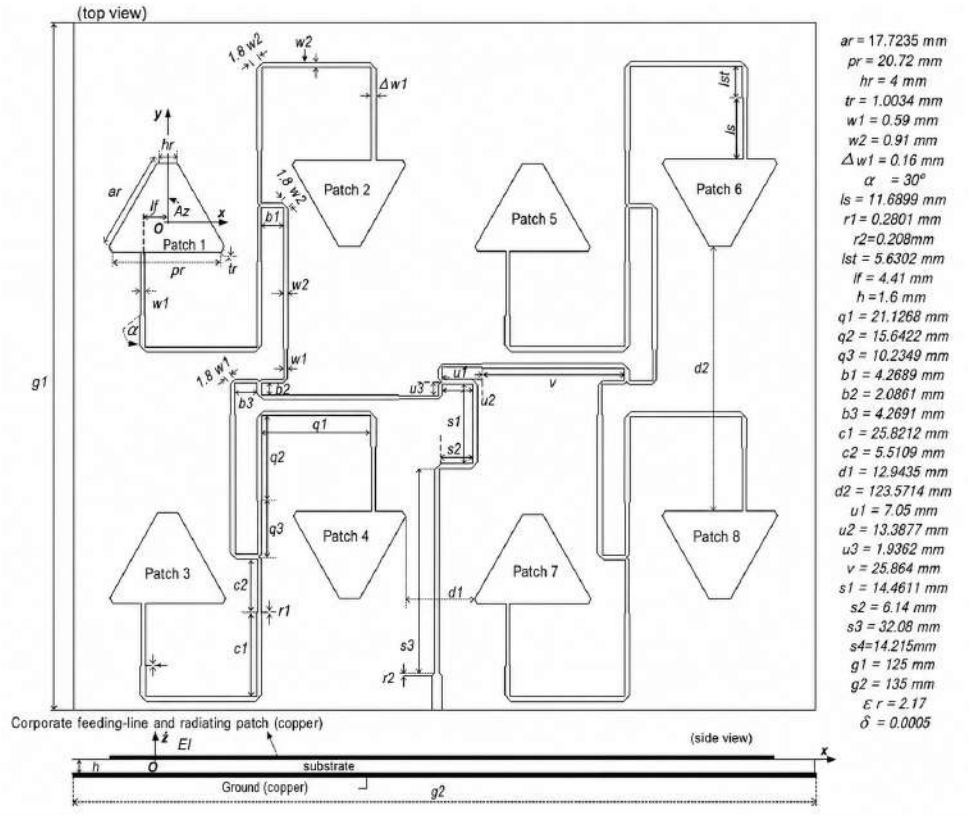

(a)

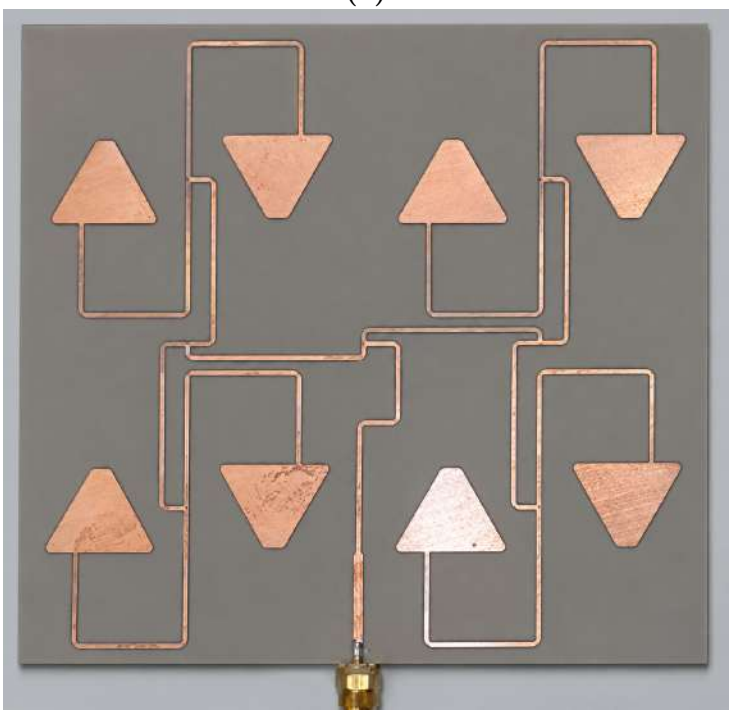

(b)

Figure 2 Construction (a) and fabrication (b) of the eight-patches array microstrip antenna

In addition to reciprocity, an ideal divider is expected to operate with minimal loss. A microwave network is considered lossless when its scattering matrix is unitary, expressed as (Delaune et al., 2006; Koo et al., 2012; Purnomo and Kitagawa, 2018; Purnomo et al., 2014; Tanaka et al., 2006):

$$[S]^T[S]^* = [I] \tag{2}$$

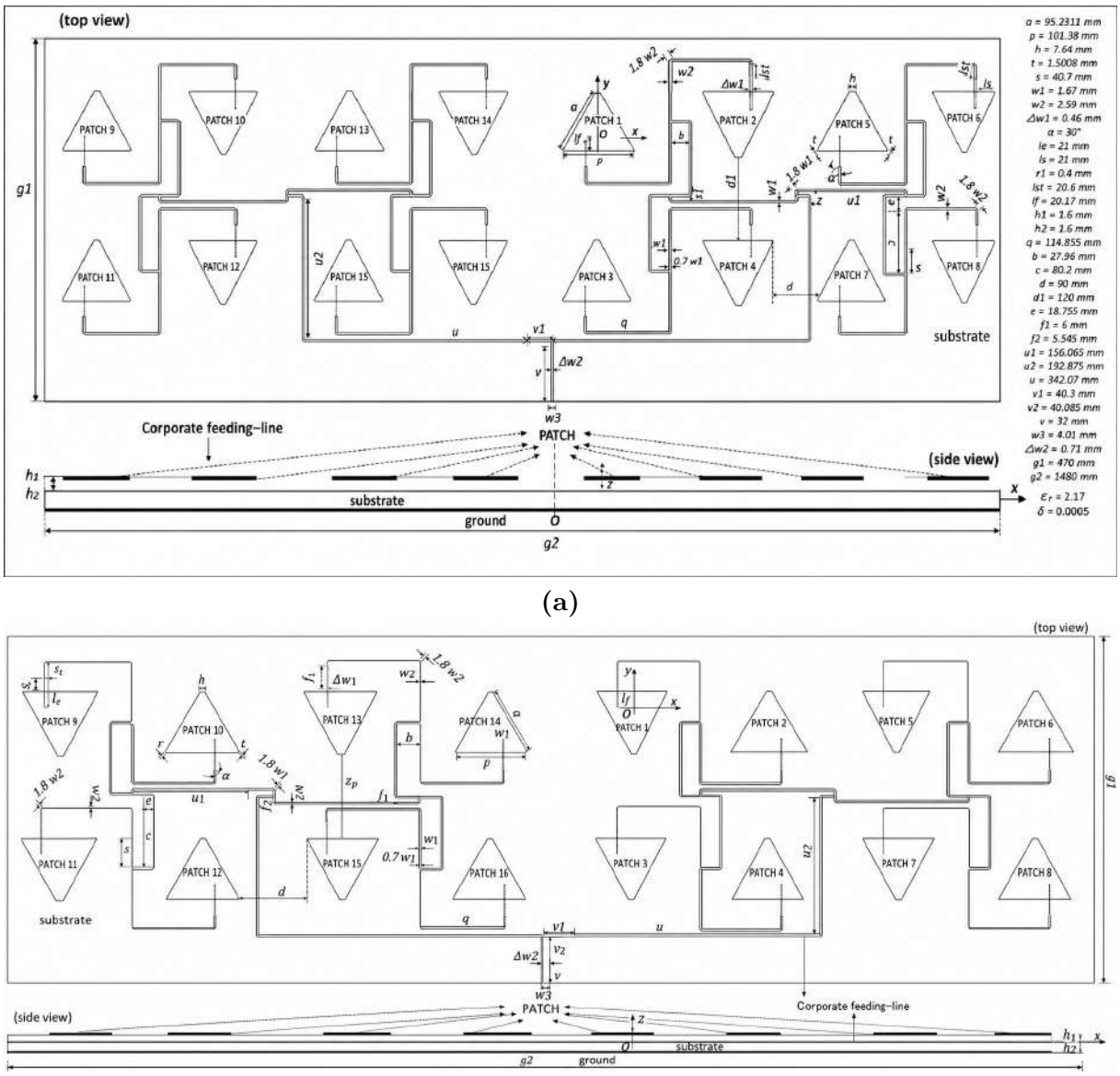

(a)

(b)

Figure 3 The LHCP (a) and RHCP (b) triangular array antenna 2×8 patches

where $[I]$ represents the identity matrix, $[S]^T$ denotes the transpose operator, and $[S]^*$ indicates complex conjugation. This condition implies that the total outgoing power equals the total incident power, with negligible dissipation inside the divider.

A −3 dB divider is theoretically defined as a passive three-port device that splits the input signal equally into two output branches. Its scattering representation can be written in matrix form as:

$$[S] = \begin{bmatrix} S_{11} & S_{12} & S_{13} \\ S_{21} & S_{22} & S_{23} \\ S_{31} & S_{32} & S_{33} \end{bmatrix} \tag{3}$$

For a matched condition at each port, the reflection coefficients S_{ii} approach zero, indicating minimal reflected power. The isolation terms S_{23} and S_{32} describe coupling between the output ports. High isolation is achieved when these parameters remain sufficiently small, ensuring that signals exiting one branch do not leak significantly into the other.

However, it has been established in microwave network theory that a three-port device cannot simultaneously satisfy perfect matching, reciprocity, and complete losslessness. As a result, practical divider designs represent an approximation of the ideal unitary behavior rather than an exact realization.

A modified 2×1 T-junction divider was used as the corporate-feed building block for the proposed array. In this work, the divider analysis was not intended as a new theoretical contribution, but as a practical design check to ensure reciprocal behavior, low reflection, and approximately equal power division between the two output branches. For this reason, only the basic scattering-matrix conditions were considered: reciprocity in Equation (1), low port reflection $S_{11} \approx 0$, and near-lossless operation as shown in Equation (2). Since an ideal reciprocal, perfectly matched, fully isolated, and strictly lossless three-port network cannot be realized simultaneously, the proposed divider was designed as a practical trade-off structure with low insertion loss and acceptable isolation. The final divider dimensions were selected from parametric sweeps of line widths, junction transitions, and bend sections, and then verified by the simulated S-matrix response at the design frequency. The extracted matrices for the LHCP and RHCP configurations showed symmetric behavior and only minor deviation from the identity condition, indicating that the divider was suitable for feeding the circularly polarized triangular patch array. This interpretation is aligned with the present draft, which already frames the divider as an approximate near-lossless implementation rather than an ideal three-port device.

2.3.1 Isolation and Lossless Constraints

Under matched-port assumptions, the scattering matrix of a three-port divider can be simplified such that the diagonal reflection terms become negligible:

$$[S] = \begin{bmatrix} 0 & S_{12} & S_{13} \\ S_{21} & 0 & S_{23} \\ S_{31} & S_{32} & 0 \end{bmatrix} \tag{4}$$

In this representation, the parameters S_{23} and S_{32} describe the isolation between the two output branches. Ideally, these coupling coefficients should be minimized to prevent signal leakage from one output port into the other.

To satisfy the lossless condition, the unitary requirement imposes strict power conservation constraints:

$$|S_{12}|^2 + |S_{13}|^2 = 1 \tag{5}$$
$$|S_{12}|^2 + |S_{23}|^2 = 1 \tag{6}$$
$$|S_{13}|^2 + |S_{23}|^2 = 1 \tag{7}$$

Additionally, orthogonality conditions must also be fulfilled (Delaune et al., 2006; Koo et al., 2012; Purnomo and Kitagawa, 2018; Purnomo et al., 2014; Tanaka et al., 2006):

$$S_{13}^* S_{23} = 0, \quad S_{23}^* S_{12} = 0, \quad S_{12}^* S_{13} = 0 \tag{8}$$

These relations imply that achieving complete isolation would require some transmission terms to approach zero. However, forcing multiple coefficients to vanish violates the power conservation equations above. Therefore, microwave theory confirms that a three-port network cannot simultaneously achieve perfect matching, reciprocity, full isolation, and lossless behavior.

Consequently, practical divider implementations represent a trade-off solution, aiming for low insertion loss and acceptable isolation rather than an ideal theoretical realization.

2.3.2 Simulated S-Matrix Verification

The scattering matrices of the proposed modified T-junction divider were extracted from CST simulations at the operating frequency of 1.25 GHz for both LHCP and RHCP configurations. The obtained matrices demonstrate symmetric characteristics, confirming reciprocal behavior:

$$[S] = [S]^T \tag{9}$$

Furthermore, the reflection coefficients at each port remain close to zero, indicating that the majority of the incident power is transmitted rather than reflected. This suggests that the divider achieves near-matched performance across its ports. To evaluate the lossless approximation, the unitary condition was examined through the matrix product:

$$[S]^T[S]^* \approx [I] \tag{10}$$

The resulting values show only minor deviations from the identity matrix, implying that the divider introduces minimal dissipative loss. Hence, both LHCP and RHCP divider structures operate as near-lossless feeding networks suitable for circularly polarized array excitation.

3. Results and Discussion

The real and imaginary parts of S-matrix for both LHCP and RHCP of the modified lossless T-junction power divider at $f = 1.25$ GHz taken from CST software are shown in Equations (11) and (12), respectively.

$$S_{\text{LHCP}} = \begin{bmatrix} 0.04 + j0.16 & 0.44 - j0.53 & 0.43 - j0.54 \\ 0.44 - j0.53 & -0.39 - j0.08 & 0.55 + j0.09 \\ 0.43 - j0.54 & 0.55 + j0.09 & -0.38 - j0.07 \end{bmatrix} \tag{11}$$

We define that $S^{\text{T}}_{\text{LHCP}}$ and S^{*}_{LHCP} are the transpose and conjugate matrix of Equation (11), respectively.

$$S_{\text{RHCP}} = \begin{bmatrix} 0.04 + j0.16 & 0.43 - j0.54 & 0.44 - j0.53 \\ 0.43 - j0.54 & -0.38 - j0.07 & 0.55 + j0.09 \\ 0.44 - j0.53 & 0.55 + j0.09 & -0.39 - j0.08 \end{bmatrix} \tag{12}$$

Also, we notice that $S^{\text{T}}_{\text{RHCP}}$ and S^{*}_{RHCP} are consecutively the transpose and conjugate matrix of Equation (12).

For reciprocity, they are clear for both LHCP and RHCP, i.e., $S_{\text{LHCP}} = S^{\text{T}}_{\text{LHCP}}$ and $S_{\text{RHCP}} = S^{\text{T}}_{\text{RHCP}}$. The matched ports of the divider set for LHCP are $S_{11} = 0.04 + j0.16$, $S_{22} = -0.39 - j0.08$, and $S_{33} = -0.38 - j0.07$; and for RHCP are $S_{11} = 0.04 + j0.16$, $S_{22} = -0.38 - j0.07$, and $S_{33} = -0.39 - j0.08$, all of which are relatively close to zero. It means that only a little bit of the incident waves on the matched port will be reflected or not exit the ports. Thus, the reflected waves at the ports will close to zero. We get that both LHCP and RHCP are almost lossless power dividers, $[S]^T[S]^* = [I]$ or $[S]^*[S]^T = [I]$, as seen in Equations (13) and (14).

$$[S]^T[S]^*_{\text{LHCP}} = \begin{bmatrix} 0.9782 & -0.0085 - j0.0022 & -0.0005 - j0.0054 \\ -0.0085 + j0.0022 & 0.9436 & 0.0384 + j0.0051 \\ -0.0005 + j0.0054 & 0.0384 - j0.0051 & 0.9364 \end{bmatrix} \approx \begin{bmatrix} 1 & 0 & 0 \\ 0 & 1 & 0 \\ 0 & 0 & 1 \end{bmatrix} \tag{13}$$

$$[S]^T[S]^*_{\text{RHCP}} = \begin{bmatrix} 0.9782 & -0.0005 - j0.0054 & -0.0085 - j0.0022 \\ -0.0005 + j0.0054 & 0.9364 & 0.0384 - j0.0051 \\ -0.0085 + j0.0022 & 0.0384 + j0.0051 & 0.9436 \end{bmatrix} \approx \begin{bmatrix} 1 & 0 & 0 \\ 0 & 1 & 0 \\ 0 & 0 & 1 \end{bmatrix} \tag{14}$$

Following the design of the corporate-fed triangular array antenna and the modified T-junction divider, a series of simulations were conducted to evaluate the antenna performance in terms of impedance matching, axial ratio, gain, beamwidth, and efficiency. Figure 4 presents the simulated reflection coefficient (S_{11}) for both LHCP and RHCP array configurations. At the resonant frequency of 1.25 GHz, the antennas exhibit return loss values of approximately -19 dB, indicating good impedance matching. The corresponding bandwidth remains around 37 MHz, which is adequate for CP-SAR operation. Figure 5 shows the frequency characteristics

of gain and axial ratio. The results confirm that the array achieves circular polarization with axial ratio values below 3 dB, while maintaining a gain level of about 7.6 dBic for the 2×1 patch configuration. As the array size increases, the gain improves significantly. For the 2×8 patch array, the simulated peak gain reaches approximately 16.5 dBic, while the axial ratio remains within the acceptable CP threshold (see Figure 6). However, when the array antenna structure is changed to a coplanar-fed array with a substrate thickness of 1.6 mm, the peak gain increases significantly to 19.5 dBic even though only eight patches are used (see Figure 7). These outcomes demonstrate that triangular microstrip arrays fed by the proposed divider network can satisfy the beamwidth and efficiency requirements of UAV-based CP-SAR systems.

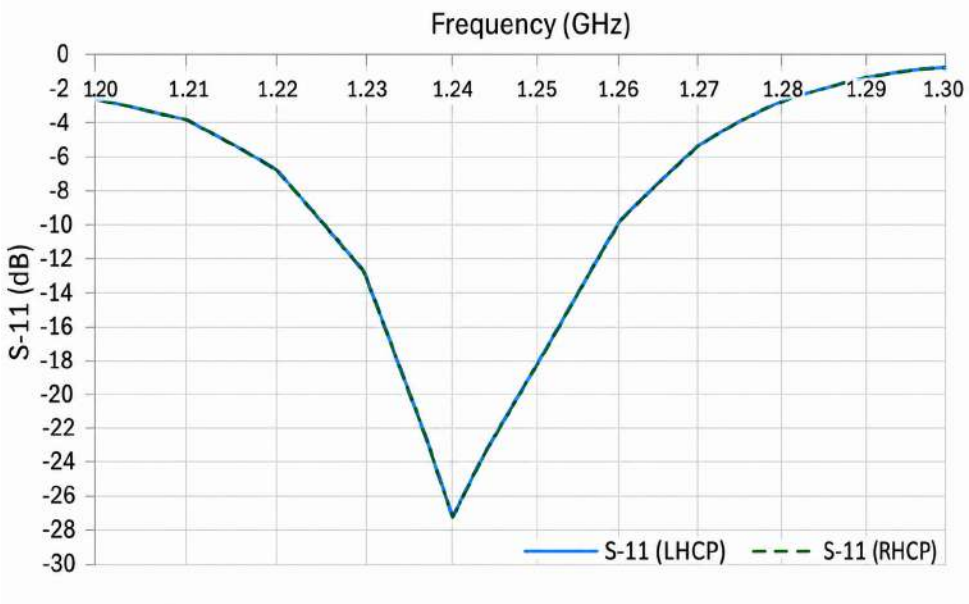

Figure 4 *S*-parameter 2×1 patch

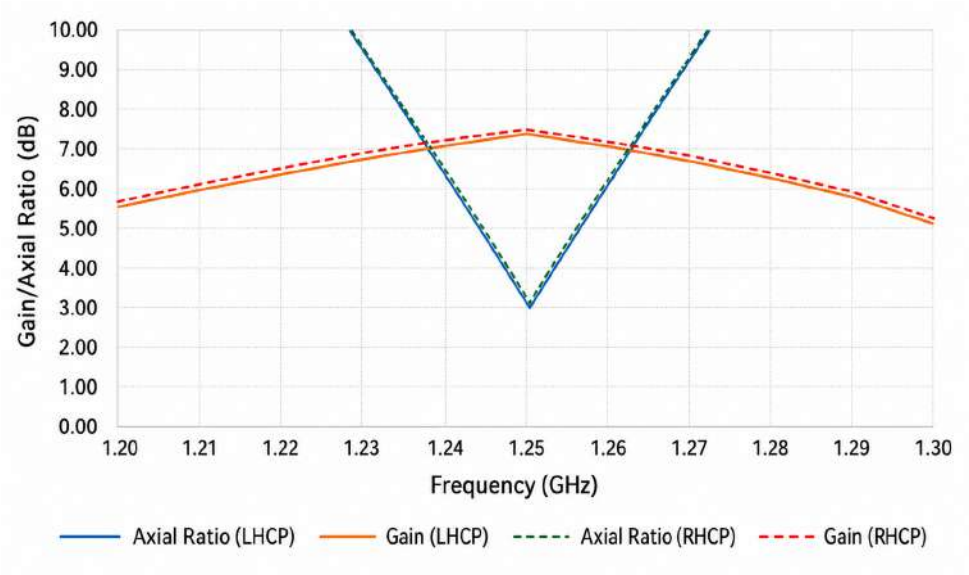

Figure 5 Axial ratio vs frequency 2×1 patch

3.1 Radiation Characteristics of 2×1 Triangular Array

The elevation and azimuth radiation characteristics of the 2×1 triangular array are illustrated in Figures 8 and 9. For both LHCP and RHCP configurations, the axial ratio remains

below 3 dB within the main radiation lobe, confirming proper circular polarization behavior. In the elevation plane (θ-plane), the 3-dB axial ratio beamwidth varies depending on the polarization orientation. For LHCP, the beamwidth spans approximately 45° in the negative-θ region and around 25° in the positive-θ region. Meanwhile, the RHCP configuration exhibits asymmetric behavior with beamwidth values of roughly 27° and 57° across opposite angular sectors. In the azimuth plane (ϕ-plane), the array demonstrates adequate coverage with axial ratio beamwidths exceeding the minimum requirement for CP-SAR applications. These results indicate that even the smaller 2×1 configuration can satisfy the basic circular polarization and beamwidth specifications.

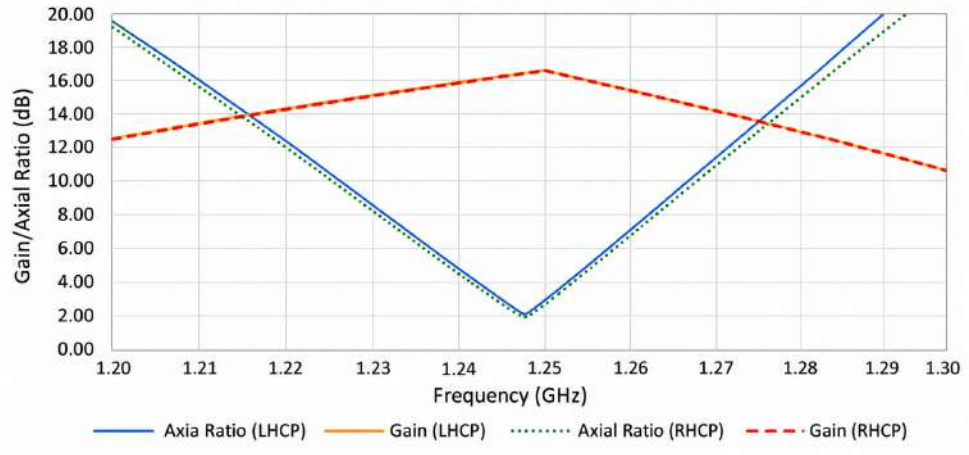

Figure 6 Frequency characteristic 2×8 patches

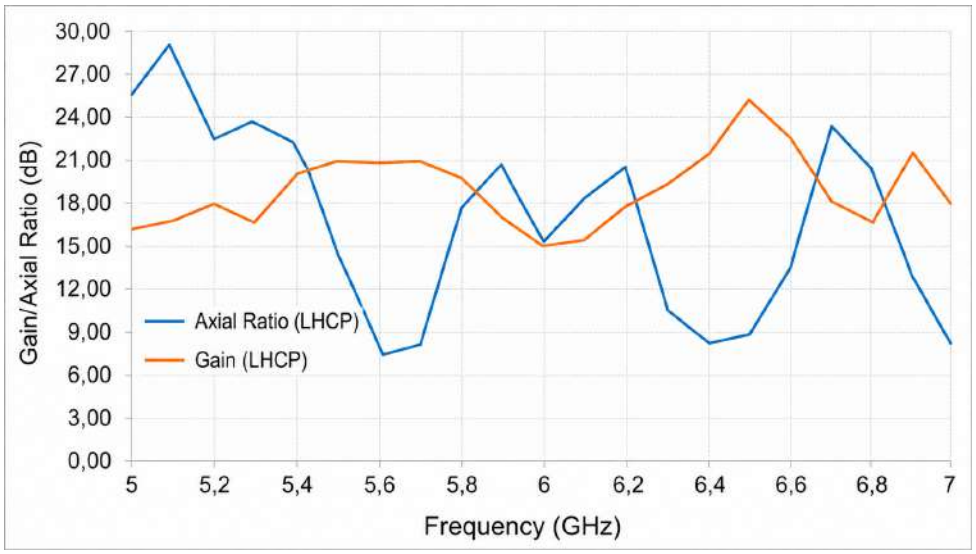

Figure 7 Frequency characteristic 2×4 patches

3.2 Performance of 2×8 Triangular Array (Sixteen Patches)

To enhance gain performance and improve directional control, the array size was expanded to a 2×8 configuration. Figure 10 presents the simulated reflection coefficient at 1.25 GHz, where both LHCP and RHCP achieve return loss values close to −20 dB. The impedance bandwidth is approximately 34 MHz, indicating stable matching performance. Figure 6 shows the frequency response of gain and axial ratio. At the operating frequency, the maximum simulated gain reaches approximately 16.5 dBic for both polarizations, while the axial ratio remains below 3 dB. Compared to the 2×1 configuration, the gain improvement is significant, demonstrating the effectiveness of array scaling. The gain bandwidth above 14 dBic extends to about 54 MHz, while

the 3-dB axial ratio bandwidth is approximately 6 MHz. Although the axial ratio bandwidth is relatively narrow, it remains sufficient for the intended CP-SAR application.

3.2.1 Elevation Plane Analysis

Figures 11 and 12 illustrate the radiation patterns in the x–z and y–z planes. The main beam is directed around ±38°, corresponding to the desired off-broadside operation for airborne SAR systems. The 14 dBic gain beamwidth in elevation is approximately 10° for both LHCP and RHCP configurations. This narrow beamwidth contributes to improved azimuth resolution in SAR imaging. Furthermore, the 3-dB axial ratio beamwidth ranges between 12° and 33°, depending on polarization orientation and observation plane. All observed values fall within the required elevation beamwidth range for UAV-based CP-SAR operation (≥15°), indicating that the sixteen-patch array fulfills directional performance targets.

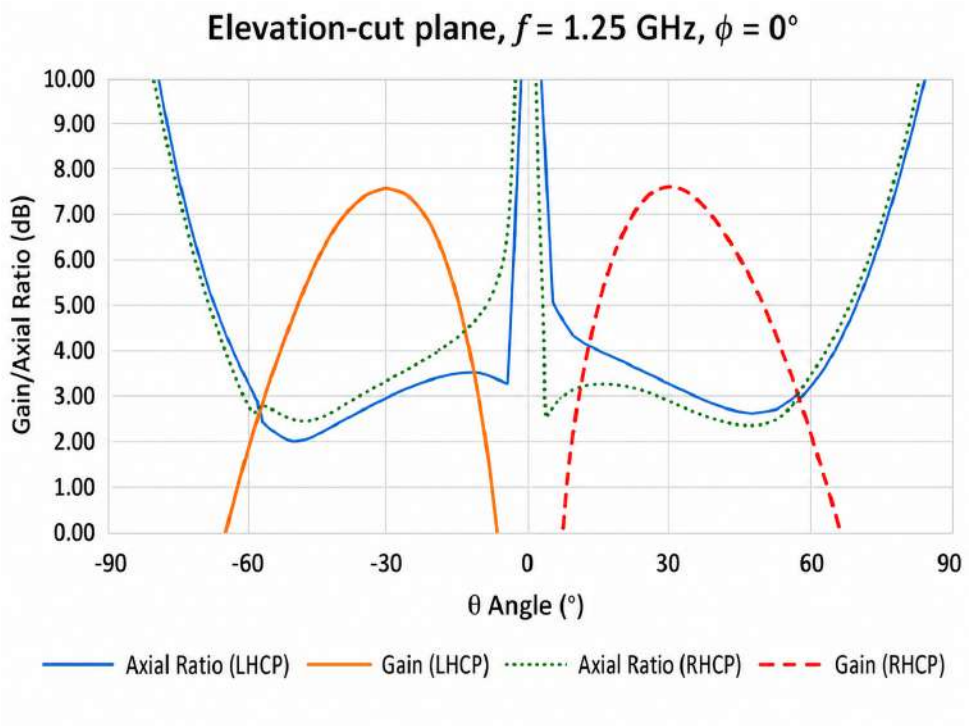

Figure 8 Elevation-cut plane 2×1 patch

3.2.2 Azimuth Plane Characteristics

Figure 13 depicts the conical radiation pattern at the operating elevation angle ($\theta \approx \pm 38°$). The maximum gain remains consistent around 16.5 dBic across principal azimuth directions ($\phi = 0°$ and 180°). The axial ratio also remains below 3 dB within the main lobe regions, confirming polarization stability. The gain beamwidth above 14 dBic spans approximately 30°–37°, while the axial ratio beamwidth extends significantly wider, reaching 70°–85° in certain angular sectors. This wide azimuthal axial ratio coverage ensures robust circular polarization performance during UAV flight maneuvers.

3.2.3 Antenna Efficiency

Figure 14 presents the radiation efficiency at the resonant frequency. The simulated efficiency values are approximately 83.6% for LHCP and 83.2% for RHCP. These results exceed the minimum target efficiency of 80% required for CP-SAR implementation. The high efficiency is primarily attributed to: (i) Low-loss substrate material ($\varepsilon_r = 2.17$, $\delta = 0.0005$); (ii) Optimized corporate feeding network; (iii) Proper element spacing and coupling compensation.

3.3 Performance of 2×4 Triangular Array (Eight Patches)

Figure 15 illustrates the simulated reflection coefficient S_{11} of the Tx/Rx eight-element microstrip antenna array. The result indicates good impedance matching over a broad frequency range, with a pronounced minimum in the upper part of the displayed band. Nevertheless, the previously stated bandwidth of 5500 MHz and the corresponding 100% fractional bandwidth are not supported by the plotted frequency axis. Based on the visible sweep of approximately 5.0–7.0 GHz, the impedance bandwidth is on the order of 2.0 GHz, corresponding to a fractional bandwidth of roughly 33–36%, depending on the adopted definition. Therefore, the proposed array exhibits a broad impedance bandwidth, but not a 100% fractional bandwidth (Nasimuddin and Esselle, 2007; Zhang et al., 2025). Figure 7 presents the simulated gain and axial ratio (AR) of the corporate coplanar-fed antenna toward $\theta = 41^\circ$ at the operational frequency. The observed gain is approximately 20.05 dBi, and the AR is measured at 12.26 dB. Although the AR value is higher than the ideal 3 dB limit for circular polarization, the gain performance is consistent with recent advances in compact, high-gain circularly polarized antennas designed for radar and telemetry systems Smith and Lee, 2023.

Figure 16 shows the measured S_{11} of the fabricated antenna. The measured resonance occurs near 6.07 GHz, with a (-10) dB bandwidth of about 126 MHz from approximately 6.00 to 6.13 GHz. This confirms good impedance matching for the measured prototype, but it also indicates a frequency shift relative to the nominal target of 5.5 GHz. Therefore, Figure 16 should be described as partial experimental validation of impedance matching for the fabricated prototype, rather than as full validation of the final CP-SAR design at 5.5 GHz. Any direct comparison between Figures 15 and 16 should explicitly acknowledge the structural and/or frequency discrepancy.

3.3.1 Elevation Plane Analysis

Figures 17 and 18 illustrate the simulation results of gain versus elevation angle (θ) as generated by the eight-element microstrip antenna array in the azimuthal (ϕ) direction for CP-SAR at a frequency of 5.5 GHz. Here, positive θ refers to the azimuth directions $\phi = 0^\circ$ and $\phi = 90^\circ$, while negative θ corresponds to $\phi = 180^\circ$ and $\phi = 270^\circ$. At an elevation angle of $\theta = 45^\circ$, the average maximum gain and axial ratio (AR) of the antenna are approximately 20.1 dBic and 12.7 dB, respectively. The 15 dBi-gain beamwidth spans 29° in the negative-θ direction, ranging from -62° to -33° ($\phi = 180^\circ$ and $\phi = 270^\circ$), and approximately 34° in the positive-θ direction, from 30° to 64° ($\phi = 0^\circ$ and $\phi = 90^\circ$). Additionally, the sidelobe level of the elevation beam remains below 13 dBi across the range. These characteristics meet the design requirements presented in Table 1, specifically: a minimum 15 dBi-gain beamwidth of $\geq$15°, and an elevation sidelobe level of $\leq$13 dBi, both of which contribute to enhanced resolution for CP-SAR applications using UAV platforms.

Figure 19 shows the measured elevation-cut radiation pattern of the eight-patch array. However, the vertical scale should not be interpreted as calibrated absolute gain in dBi. If the plotted quantity is a normalized receiver level, relative field strength, or uncalibrated pattern magnitude, it should be relabeled accordingly. Claiming a maximum gain of 35 dB for an eight-element passive microstrip array is not physically well supported and is inconsistent with typical gains reported for comparable circularly polarized microstrip arrays. Hence, Figure 19 is more appropriately discussed as demonstrating the shape of the elevation radiation pattern, including the main lobe and side lobes, rather than absolute gain.

3.3.2 Azimuth Plane Characteristics

Figure 20 illustrates the simulation result of the azimuth plane radiation pattern at an elevation angle of $\theta = 41^\circ$ for left-hand circular polarization (LHCP) at a frequency of 5.5 GHz. On this plane, the maximum gain is 20.05 dBi at $\phi = 0^\circ$, while the minimum axial ratio (AR) is 2.25 dB at $\phi = 215^\circ$. The primary 15 dBi-gain beamwidths observed on the x–y plane is

approximately 52°, spanning from $\phi = 334°$ to $\phi = 26°$, and about 30°, ranging from $\phi = 170°$ to $\phi = 200°$. Furthermore, the sidelobe level on the x–y plane remains below 12 dBi. These results demonstrate that the antenna satisfies the targeted azimuthal beamwidth requirement of $\geq$15° at 15 dBi gain and maintains a sidelobe level of $\leq$13 dBi, as outlined in the CP-SAR UAV resolution criteria.

Figure 21 displays a polar plot of antenna gain as a function of the azimuthal angle (ϕ) at a fixed elevation angle of $\theta = 45°$, for a microstrip antenna without parasitic patches. This type of plot is useful for visualizing how the antenna radiates energy in different horizontal directions. From the plot, the gain pattern is asymmetric, indicating a directional preference in the azimuth plane. The maximum gain is observed around $\phi = 0°$, reaching nearly 25 dB, while other directions show significantly lower values, some dropping below 10 dB. This suggests the antenna has a highly directional radiation pattern at this specific cut, favoring forward radiation over side or back lobes. Overall, the gain versus ϕ plot at $\theta = 45°$ confirms that the antenna provides strong forward gain, with minimal omnidirectional characteristics. Introducing parasitic elements in a follow-up design could be used to reshape the pattern — either to enhance directionality further or to broaden the beam, depending on the application.

4. Conclusions

This study has presented the design and evaluation of triangular microstrip array antennas intended for Circularly Polarized Synthetic Aperture Radar (CP-SAR) applications operating at 1.25 GHz (sixteen-patch) and 5.5 GHz (eight-patch). The triangular geometry was selected because of its compact configuration and suitability for planar array integration, enabling simultaneous transmitter (Tx) and receiver (Rx) implementation within a unified structure. A corporate-fed architecture combined with a modified T-junction power divider was employed to achieve balanced excitation across the radiating elements. Theoretical analysis of the scattering matrix confirmed that although an ideal three-port network cannot simultaneously satisfy perfect matching, reciprocity, and complete losslessness, the proposed divider closely approximates near-lossless and reciprocal behavior. Performance evaluation demonstrated that the sixteen-patch (2×8) triangular array achieves a peak gain of approximately 16.5 dBic while maintaining axial ratio values below 3 dB at the operating frequency. The elevation beamwidth and azimuth characteristics satisfy the directional requirements for UAV-based CP-SAR systems. In addition, the simulated radiation efficiency exceeds 83%, surpassing the minimum design target of 80%. Meanwhile, the eight-patch (2×4) triangular array obtains the peak gain increasing significantly to 19.5 dBic. This is because the antenna array structure is changed to a coplanar-fed array with a substrate thickness of 1.6 mm. These results confirm that triangular microstrip array antennas with truncated-tip perturbation and corporate feeding networks provide a feasible and efficient solution for compact CP-SAR platforms deployed on UAVs and LEO microsatellites. Future work may focus on bandwidth enhancement techniques and experimental validation of the full-scale array prototype CP-SAR using aircraft.

Acknowledgements

The authors would like to express their gratitude to Board of Research and Community Service (BPPM), Faculty of Engineering (Number 1351 Year 2025), PPKID (010/UN10.C10.18/PN/2022), and WCU Brawijaya University (Number: 1/UN10.WCU/LL/2023), Malang, Indonesia for the funding of this publication. Also, special thanks to Board of Research and Innovation Nation (BRIN), Bogor and Bandung, West Java, Indonesia and the Center for En-vironmental Remote Sensing, Chiba University, Chiba, Japan, for facilitating CST Studio Suite Software and other equipment for the support to collect the data in this research.

Author Contributions

Conceptualization, methodology: M.F.E.P and V.K.; software: M.F.E.P, A.Z., and D.F.K.; validation: F.H.P, S.K., and R.R.; formal analysis: M.F.E.P and M.A.M; investigation: H.S; resources: R.N.H; writing—original draft preparation: F.K., M.F.E.P., and J.T.S.S; writing—review and editing: P.D.P.A., B.S., M.F.E.P, K.A, and N.N; visualization: F.H.P; project administration: V.K.

Conflict of Interest

The authors declare no conflicts of interest.

Supplementary Materials

There are no supplementary materials.

Declaration of AI

The authors declare that generative AI or AI-assisted technologies were used in the preparation of this manuscript and references using Harvard referencing style. All content, including text, figures, data analysis, and conclusions, was produced solely by the authors.

References

Amr, H. H., Mohamed, A. M., & Haythem, H. A. (2017). Hardware implementation of antenna array system for maximum SLL reduction. *Engineering Science and Technology, an International Journal*, *20*(3), 965–972. https://doi.org/10.1016/j.jestch.2016.11.014

Ansoft Corporation. (2001). ANSOFT ensemble user guide manual (ver. 8).

Asfour, R., Khamas, S., Ball, E., Ng, J., Huang, G., Allanic, R., Le Berre, D., Quendo, C., Leuliet, A., & Merlet, T. (2024). On-chip circularly polarized circular loop antennas utilizing 4h-sic and gaas substrates in the q/v band. *Sensors*, *24*(2), 321. https://doi.org/10.3390/s24020321

Baharuddin, M., Wissan, V., Sri Sumantyo, J. T., & Kuze, H. (2009). Equilateral triangular microstrip antenna for circularly-polarized synthetic aperture radar. *Progress in Electromagnetics Research C*, *8*, 107–120. https://doi.org/10.2528/PIERC09052202

Basari, Sri Sumantyo, J. T., Takahashi, M., & Ito, K. (2006). Circularly polarized triangular microstrip array antenna using single-fed proximity-coupled for mobile satellite communications applications. *Proceeding IJJSS 2006*.

Beegum, S., Joseph, M., Joyas, S., Jayakumar, M., & Girija, J. (2024). Dual circularly polarized broadband microstrip antenna array for space re-entry vehicle applications in s band. *ICTACT Journal on Communication Technology*, *15*(3), 3229–3235. https://doi.org/10.21917/ijct.2024.0481

Chang, K. (2005). *Encyclopedia of RF and microwave engineering*. John Wiley & Sons Inc.

Chen, Q., Yang, J., He, C., Zhang, D., Huang, S., Wang, M., Yu, F., & Dai, G. (2024). Wideband circularly polarization and high-gain of a slot patch array antenna realized by a hybrid metasurface. *Sensors*, *24*(11), 3510. https://doi.org/10.3390/s24113510

CST AG. (2016). CST STUDIO SUITE 2016: Microwave–radio frequency–optical [Copyright © 1998–2016 CST AG].

Delaune, D., Sri Sumantyo, J. T., Takahashi, M., & Ito, K. (2006). Circularly polarized rounded-off triangular microstrip line array antenna. *IEICE Transactions on Communications*, *E89-B*(4), 1372–1381.

Delfini, D., Tervo, N., Javed, M., Leinonen, M., & Pärssinen, A. (2024). Tapering impact on the spatial and frequency responses of broadband asymmetrically routed phased arrays. *2024 18th European Conference on Antennas and Propagation (EuCAP)*, 1–5. https://doi.org/10.23919/EuCAP60739.2024.10501642

Deshmukh, A., & Ray, K. (2020). Circularly polarized designs of modified isosceles triangular microstrip antennas. *Engineering Reports*, *2*(10). https://doi.org/10.1002/eng2.12250

Deshmukh, A. A., & Chavali, V. A. P. (2026). Reconfigurable designs of u-slot cut microstrip antennas for dual band circularly polarized response. *Progress In Electromagnetics Research B*, *116*, 1–18. https://doi.org/10.2528/PIERB25072205

Ding, Z., Xu, M., Li, X., Tao, S., Wang, H., & Zhang, X. (2023). Design of wideband circularly polarized metasurface antenna using characteristic mode analysis. *Microwave and Optical Technology Letters*, *65*(6).

Dong, G., Lv, S., & Zhang, Y. (2025). A Ku-band circularly polarized array antenna based on vertical virtual ground. *Electronics*, *14*(23), 4691. https://doi.org/10.3390/electronics14234691

Du, B., & Yung, E. K. N. (2002). Single-feed TM21 mode circular patch antenna with circular polarization. *Microwave and Optical Technology Letters*, *33*(3), 154–156. https://doi.org/10.1002/mop.10262

Grebennikov, A. (2011). *RF and microwave transmitter design*. John Wiley & Sons Inc.

Horng, T. S., & Alexopoulos, N. G. (1993). Corporate feed design for microstrip arrays. *IEEE Transactions on Antennas and Propagation*, *41*(12), 1615–1624. https://doi.org/10.1109/8.273304

Ishihara, H., Yamamoto, A., & Ogawa, K. (2002). A simple model for calculating the radiation patterns of antennas mounted on a vehicle roof. *Interim International Symposium on Antenna and Propagation*, 548–551.

Jiao, Y., Zhang, F., Liu, X., Huang, Z., & Yuan, J. (2025). C-SAR/02 satellite polarimetric calibration and validation based on active radar calibrators. *Remote Sensing*, *17*(2), 282. https://doi.org/10.3390/rs17020282

Kashihara, H., Sumantyo, J. T. S., Izumi, Y., Ito, K., Gao, S., & Namba, K. (2023). X-band microstrip array antenna for UAV onboard full circularly polarized synthetic aperture radar. *IEEE Transactions on Antennas and Propagation*, *71*, 1943–1948.

Kedze, K., Wang, H., Park, Y., & Park, I. (2022). Substrate dielectric constant effects on the performances of a metasurface-based circularly polarized microstrip patch antenna. *International Journal of Antennas and Propagation*, *2022*, 3026677. https://doi.org/10.1155/2022/3026677

Koo, V. C., Chan, Y. K., Vetharatnam, G., Chua, M. Y., Lim, C. H., Lim, C. S., Thum, C. C., Lim, T. S., Ahmad, Z., Mahmood, K. A., Shahid, M. H., Ang, C. Y., Tan, W. Q., Tan, P. N., Yee, K. S., Cheaw, W. G., Boey, H. S., Choo, A. L., & Sew, B. C. (2012). A new unmanned aerial vehicle synthetic aperture radar for environmental monitoring. *Progress in Electromagnetics Research*, *122*, 245–268. https://doi.org/10.2528/PIER11092604

Li, M., Sun, Z., Tang, M.-C., & Zhu, L. (2024). Broadband circularly polarized microstrip antenna with customized tilted beam based on index-modulated folded split ring resonator. *IEEE Transactions on Antennas and Propagation*, *72*(3), 2831–2836. https://doi.org/10.1109/TAP.2024.3353346

Li, Z., Liu, Y., Zhao, M., Zong, W., & He, S. (2025). A wideband circularly polarized metasurface antenna with high gain using characteristic mode analysis. *Electronics*, *14*(14), 2818. https://doi.org/10.3390/electronics14142818

Liu, S., Yang, L., & Wu, X. (2022). A low-profile wideband circularly polarized metasurface antenna based on characteristic mode theory. *Applied Computational Electromagnetics Society Journal*, *37*(11), 1110–1117. https://doi.org/10.13052/2022.ACES.J.371101

Morini, A., Rozzi, T., Farina, M., & Angeletti, P. (2024). Scattering matrix of a reciprocal and lossless, three-port power divider. *IEEE Microwave and Wireless Technology Letters*, *34*(11), 1223–1226. https://doi.org/10.1109/LMWT.2024.3460168

Mujahidin, I., Pramono, S. H., & Muslim, A. (2018). 5.5 GHz directional antenna with 90 degree phase difference output. *Proceedings of the 2018 Electrical Power, Electronics,*

Communications, Controls, and Informatics Seminar (EECCIS), 224–228. https://doi.org/10.1109/EECCIS.2018.8692872

Nasimuddin & Esselle, K. P. (2007). High-gain wideband circularly polarized stacked microstrip antennas with single microstrip feeds and short horns. *Proc. IEEE Antennas and Propagation Society Int. Symp.*, 737–740.

Park, M. Y., Kim, J. H., Yi, S. H., Lim, W., Yang, Y., & Hwang, K. C. (2024). Design of series-fed circularly polarized beam-tilted antenna for microwave power transmission in UAV application. *Applied Sciences*, *14*, 3490. https://doi.org/10.3390/app14083490

Pozar, D. (2005). *Microwave engineering* (3rd). John Wiley & Sons Inc.

Purnomo, M. F. E., Basari, & Sri Sumantyo, J. T. (2014). Circularly polarized stack-patch microstrip array antenna for mobile satellite communications. *Proceedings IJJSS 2014, Theme Antenna and Microwave*, 269–275.

Purnomo, M. F. E., & Kitagawa, A. (2017). Developing basic configuration of triangle array antenna for circularly polarized-synthetic aperture radar sensor application. *Proceedings of IEEE 2017 International Conference on Radar, Antenna, Microwave, Electronics, and Telecommunications (ICRAMET 2017)*, 112–117.

Purnomo, M. F. E., & Kitagawa, A. (2018). Analysis performance of triangle microstrip antenna for basic construction of circularly polarized-synthetic aperture radar application. *Jurnal Teknologi*, *80*(2). https://doi.org/10.11113/jt.v80.11119

Purnomo, M. F. E., Kusumasari, V., Ambarwati, R., Supriana, E., Yuwono, R., Adi, P. D. P., & Kitagawa, A. (2021). Development of patch stack antenna for CP-SAR sensor. *Bulletin of Electrical Engineering and Informatics*, *10*(1), 200–207. https://doi.org/10.11591/eei.v10i1.2672

Purnomo, M. F. E., Kusumasari, V., Supriana, E., Ambarwati, R., & Kitagawa, A. (2020). Development of triangular array eight patch antennas for circularly-polarized synthetic aperture radar sensor. *TELKOMNIKA (Telecommunication, Computing, Electronics and Control)*, *18*(2), 631–639. https://doi.org/10.12928/TELKOMNIKA.v18i2.14759

Purnomo, M. F. E., Kusumasari, V., Suyono, H., Hasanah, R. N., & Kitagawa, A. (2019). The four patches of triangular microstrip antennas as configuration of CP-SAR. *Proceedings of the 2019 2nd International Conference on Electronics and Electrical Engineering Technology (EEET 2019)*, 55–61. https://doi.org/10.1145/3362752.3362768

Purnomo, M. F. E., Pramono, S. H., Pamungkas, M. A., & Taufik. (2015). Study of the effect of air-gap on array microstrip antenna performances for mobile satellite communications [ISSN 1819-6608]. *ARPN Journal of Engineering and Applied Sciences*, *10*(20).

Purnomo, M. F. E., & Sri Sumantyo, J. T. (2011). Design circularly polarized of equilateral triangular hole antenna for SAR (synthetic aperture radar) [ISSN 0913-5685]. *IEICE Technical Report*, *111*(239).

Reis, S., Silva, F., Albuquerque, D., & Pinho, P. (2025). General overview of antennas for unmanned aerial vehicles: A review. *Electronics*, *14*, 3205. https://doi.org/10.3390/electronics14163205

Sahana, K., & Sowmya, K. (2024). Planar rectangular microstrip patch antenna array with corporate-feed network for gain enhancement. *International Journal for Research in Applied Science and Engineering Technology*, *12*(8), 108–112. https://doi.org/10.22214/ijraset.2024.63863

Sarkar, T. K., Djordjevic, A. R., & Kolundzija, B. M. (2000). *Method of moments applied to antennas*. MTT ETF BGAC.

Smith, J. A., & Lee, R. B. (2023). A wideband stacked microstrip patch antenna for telemetry applications. *International Journal of Antennas and Propagation*, *2023*, 604303.

Tanaka, T., Houzen, T., Takahashi, M., & Ito, K. (2006). Circularly polarized printed antenna combining slots and patch. *IEICE Transaction Communications*, *E89-B*.

Tiwari, A., Yilmaz, M. Y., Soni, G. K., & Yadav, D. (2025). Design and development of multi-band multi-mode frequency reconfigurable CPW-fed antenna for 5G wireless communi-

cation. *International Journal of Reconfigurable and Embedded Systems (IJRES)*, *14*(2), 328–338. https://doi.org/10.11591/ijres.v14.i2.pp328-338

Tran-Huy, H., & Pham-Danh, T. (2025). Low-profile high-gain circularly polarized antenna using high-order mode microstrip patch. *Heliyon*, *11*(9), e42863.

Urata, K. N., Sumantyo, J. T. S., Perissin, D., & Viscor, T. (2019). A compact C-band CP-SAR microsatellite antenna for earth observation. *Acta Astronautica*, *159*, 517–526.

Wahyudi, Setyadewi, I. T., Sakti, M. A. K., Prabowo, Y., Hadiyanti, D. M., Rahayu, N., Muzayadah, N. L., Wahyudi, A. H., Guno, Y., Praludi, T., Santosa, C. E., & Sri Sumantyo, J. T. (2025). Analysis of unmanned aerial vehicle airframe materials on circularly polarized antenna radiation characteristics. *Bulletin of Electrical Engineering and Informatics*, *14*(4), 2649–2661. https://doi.org/10.11591/eei.v14i4.8010

Wong, K. L. (2002). *Compact and broadband microstrip antennas*. Wiley.

Yohandri, Y., Wissan, V., Firmansyah, I., Rizki Akbar, P., Sri Sumantyo, J. T., & Kuze, H. (2011). Development of circularly polarized array antenna for synthetic aperture radar sensor installed on UAV. *Progress in Electromagnetics Research C*, *19*, 119–133. https://doi.org/10.2528/PIERC10121708

Zhang, Y., Wang, Y., & Li, X. (2025). Low-profile high-gain circularly polarized antenna using high-order mode. *Heliyon*, *11*(3), e01244.